X^- (X = O, S) Ions in Alkali Halide Lattices through Density Functional Calculations. 1. Substitutional Defect Models

F. Stevens,[†,‡] H. Vrielinck,[†] V. Van Speybroeck,[‡] E. Pauwels,[‡] F. Callens,[†] and M. Waroquier*[,‡]

Department of Solid State Sciences, Ghent University, Krijgslaan 281-S1, B-9000 Ghent, Belgium, and Center for Molecular Modeling, Laboratory of Theoretical Physics, Ghent University, Proeftuinstraat 86, B-9000 Ghent, Belgium

Received: December 2, 2005; In Final Form: February 9, 2006

Monoatomic X^- (X = O, S) chalcogen centers in MZ (M = Na, K, Rb and Z = Cl, Br, I) alkali halide lattices are investigated within the framework of density functional theory with the principal aim to establish defect models. In electron paramagnetic resonance (EPR) experiments, X^- defects with tetragonal, orthorhombic, and monoclinic *g*-tensor symmetry have been observed. In this paper, models in which X^- replaces a single halide ion, with a next nearest neighbor and a nearest neighbor halide vacancy, are validated for the X^- centers with tetragonal and orthorhombic symmetry, respectively. As such defect models are extended, the ability to reproduce experimental data is a stringent test for various computational approaches. Cluster in vacuo and embedded cluster schemes are used to calculate energy and EPR parameters for the two vacancy configurations. The final assignment of a defect structure is based on the qualitative and quantitative reproduction of experimental *g* and (super)hyperfine tensors.

1. Introduction

Although defects introduced by chalcogen doping in alkali halide MZ (M = Na, K, Rb and Z = Cl, Br, I) lattices have already been studied since the late 1950s, the discovery of superfluorescence of diatomic XY^- (X,Y = O, S, Se) molecular ions in MZ lattices[1,2] has stimulated recent experimental and theoretical interest.[3−11] Among the different experimental techniques applied to investigate these defects, electron paramagnetic resonance (EPR),[12−28] electron nuclear double resonance (ENDOR),[29−33] and photoluminescence[34−39] have been used extensively. For the apparently simple monoatomic X^- chalcogen defects, which are the subject of the present study, no final microscopic models could be assigned yet, in contrast to the di- and triatomic centers. For the latter centers, we were able to calculate the EPR and ENDOR parameters using density functional theory (DFT) quite successfully,[6−11] showing that theoretical calculations can make an important contribution to the understanding of the measured EPR data. *The principal aim of the present work is to interpret the available EPR data on monoatomic chalcogen centers in alkali halide lattices by cross referencing with theoretical calculations and to assign the appropriate defect models.*

On the basis of experimental results, a distinction has been made between X^- centers wherein the chalcogen ion occupies a substitutional or an interstitial position in the lattice.[28] In this paper, attention is focused on defects where the chalcogen ion was proposed to be located substitutionally. These defects have either tetragonal ($g_{||}$ along a ⟨100⟩ direction) or orthorhombic-I (g_x, g_y, and g_z along $\langle\bar{1}10\rangle$, ⟨001⟩, and ⟨110⟩ directions) *g*-tensor symmetry according to various experimental papers.[18,19,21] The study of the centers with monoclinic symmetry, for which an interstitial location of the chalcogen ion has been suggested, is presented in paper 2.

The symmetry of the centers under study can only be explained if a lattice imperfection in the vicinity of the substitutional X^- ion is considered. As further motivated in section 2, we assume that this imperfection is a halide vacancy in a nearest neighbor (nn) or next nearest neighbor (nnn) position for the centers with orthorhombic-I and tetragonal symmetry, respectively. Such defect structures are quite extended and remain therefore a challenge for current computational techniques, as large parts of the system need to be taken into consideration to properly account for relaxations around the anion vacancy.

All commonly used approximation schemes for treating defects in ionic lattice environments fall in three categories: the cluster in vacuo approach, the embedded cluster model, and the periodic approximation.

The defect model which is finally retained for a given impurity center must be able to reproduce the experimentally determined *g* and (super)hyperfine tensors. As shown in ref 9, an accurate prediction of the *g* tensor is not always straightforward. Moreover, we deal with systems for which the *g* value deviates largely from the free electron value, that is, $\Delta g = g - g_e$ is ranging from 0.1 to 0.7. Such cases have only been scarcely addressed in the literature.[40−43] Therefore, the quantum mechanical description of the defects under consideration is a great challenge for the present DFT methods. In those cases where the quantitative agreement is less satisfactory, qualitative trends may be used to validate the proposed defect structure.

In addition, also energetic considerations should be taken into account: one may expect a pronounced influence of the vacancy position on the energy of the defect structure. This study should be made very carefully, as calculated binding energies are very sensitive to the adopted cluster approach (size of the quantum mechanical cluster, embedding scheme, etc.). These energetic aspects are extensively investigated in the KCl:S^- case. This

* To whom correspondence should be addressed. Tel: +32-9-264.65.59. Fax: +32-9-264.66.97. E-mail: michel.waroquier@UGent.be.
† Department of Solid State Sciences, Ghent University.
‡ Laboratory of Theoretical Physics, Ghent University.

10.1021/jp057008l CCC: $33.50
Published on Web 04/05/2006

research is related to the work of Aguado et al.[44,45] and Bannon et al.,[46,47] who have studied the lowest energy vacancy configuration for di- and trivalent cations in alkali and silver halides.

This paper is structured as follows. Experimental observations concerning the tetragonal and orthorhombic X^- centers are discussed in section 2, where our choice of defect models is also motivated. In section 3, the computational details are summarized and the various clusters which are used in this work are introduced. A brief overview of all simulation schemes is also given. In section 4, a suitable computational approach is selected by performing cluster in vacuo and embedded cluster calculations on the KCl:S^- test case. Extension is made to all other MZ:X^- systems in section 5. The most important results are summarized in section 6.

2. Experimental Section: Observations and Defect Models

X^- defects only appear in chalcogen-doped alkali halides after irradiation (X-ray or UV) and are stable at room temperature. The observation of a hyperfine structure with a single ^{17}O, ^{33}S (isotopically enriched dopants), or ^{77}Se (natural abundance 7.6%) in their EPR spectra identified them as monoatomic chalcogen centers. Their spin ($S = {}^1/_2$) and g tensors are characteristic for paramagnetic ions with an $(np)^5$ electron configuration.[21] They have been found in three symmetry varieties. Only O^- centers have been observed to exhibit tetragonal g-tensor symmetry.[19,20,22] In the KCl, KBr, and RbI lattices, a superhyperfine interaction with one alkali ion was resolved in the EPR spectra, identifying their symmetry as C_{4v}. Several S^- defects[18] and one O^- (in KBr)[22] have been found with orthorhombic-I g-tensor symmetry. For the latter, a small monoclinic distortion could not be excluded. O^-, S^-, and Se^- centers with monoclinic-I symmetry, that is, with one principal g axis along a $\langle 110\rangle$ direction and the other two tilted away from $\langle 001\rangle$ and $\langle \bar{1}10\rangle$ in a {110} plane, have all been encountered. It is worth noting that for some MZ:X^- systems two symmetry variants have been reported but never in the same crystal.

For paramagnetic ions with an $(np)^5$ electron configuration, a Jahn−Teller distortion[48] is expected to lift the orbital degeneracy and lower the symmetry from cubic to tetragonal or trigonal, corresponding to D_{4h} or D_{3d} for a substitutional and D_{2d} or C_{3v} for an interstitial X^-. The experimentally observed centers have lower symmetry, implying that an additional nearby lattice imperfection is present. As widely different crystal growth conditions gave rise to only the aforementioned three X^- defect structures, it is reasonable to assume that this additional imperfection is of an intrinsic nature. Upon doping, the chalcogen ions are assumed to be incorporated as diamagnetic X^{2-} ions. For substitutional incorporation, local charge compensation may be preserved by an nn or an nnn halide vacancy. Hole trapping after X-ray or UV irradiation would thus produce X^- centers with orthorhombic-I (C_{2v}) and tetragonal (C_{4v}) symmetries, respectively, corresponding to two of the observed symmetry varieties. These models are illustrated in Figure 1. Although a substitutional X^- in alkali halides does not require charge compensation, the presence of a vacancy may still be energetically favorable, for example, by reducing stress in the lattice induced by doping. Therefore, an already present vacancy may remain bound to the defect, even after hole trapping. In the present paper, the validity of these two models for the X^- centers, for which in the literature a substitutional position for the chalcogen ion has been proposed, is examined. The monoclinic-I centers, which have been tentatively identified as X^- ions at a distorted interstitial site, are the subject of a separate paper (hereafter called 2).

3. Computational Details and Selection of Clusters

All calculations in this paper were performed using either the Amsterdam Density Functional (ADF) program package, version 2004[49] or the Gaussian03 (G03) package.[50] All geometry optimizations for the cluster in vacuo approach were performed using the ADF program, relaxing the nearest four lattice shells around the substitutional X^- ion. The choice of G03 in some cases is motivated by the extended possibilities of embedding making possible an optimization of a quantum cluster in an array of fixed point charges. Also, a three-layered embedding scheme developed by Sushko and co-workers,[51,52] that is, the GUESS program which has an interface with G03, was used in this work. For these calculations, Buckingham-type interatomic potentials, developed by van Beest et al.,[53,54] were used.

All optimizations in ADF were performed using a TZP (triple-ζ plus additional polarization function) basis set and the VWN[55] functional. The subsequent EPR calculations were performed using the Bp86[56,57] functional and a TZ2P (triple-ζ plus two polarization functions) basis set. These choices are based on an earlier level of theory study on magnetic resonance parameters of chalcogen XY^- defects in alkali halides.[9] The relativistic atomic potentials were calculated using the auxiliary program DIRAC,[58] as comprised in the ADF package. For the calculation of g tensors, a spin−orbit relativistic restricted open shell approach, and for the calculation of hyperfine tensors, a scalar relativistic unrestricted approach, have been used. The frozen core approximation was applied for all ions (Na 2p, K 3p, Rb 3p, Cl 2p, Br 3p, and I 4d) except for the central ion and the nearest lattice ions.[7] In this notation, Na 2p means that all electrons up to the 2p electron shell were kept frozen.

All calculations in G03 were performed at a spin unrestricted level of theory. Similar to the ADF calculations, the VWN[55] functional form is used throughout all geometry optimizations and the Bp86[56,57] functional is applied for all subsequent EPR calculations. A 6-31G** basis set[59] was used for all atoms of the lattice environment, while a 6-311G** basis set[59] was applied for the central impurity ion.[9]

3.1. Definition of Clusters. In this subsection, the composition of the various clusters suitable for substitutional defect models and the nomenclature which will be used throughout this paper is introduced. In a substitutional model, a lattice shell is composed of either alkali or halide ions. In Table 1, the first shells of cation (M^+) and anion (Z^-) neighbors around a halide lattice position are defined. All clusters used in this work consist of complete shells. The following minimum criteria must be fulfilled to retain a cluster in vacuo: (i) the total charge must be minimal, (ii) the electrostatic potential at the halide vacancy must be well reproduced (Madelung constant: 1.74758 for infinite KCl type lattices[60]),[6] and (iii) it should contain the nn and nnn halide positions where vacancies are considered.

The smallest cluster fulfilling these criteria contains 32 neighboring atoms that are members of the first four shells. During the rest of the paper, a given cluster is always denoted with the total number of regular lattice positions it contains, thus including the central anion position. In the 33 cluster, the nnn vacancy is located at the edge of the quantum cluster and the geometry relaxation of such a configuration could lead to incorrect results, as will be shown in section 4. Other clusters that fulfill the minimum criteria are the 87, 125, 185, and 403 clusters. Their shell composition (SC), total charge (Q), and Madelung constant (MC) are summarized in Table 2.

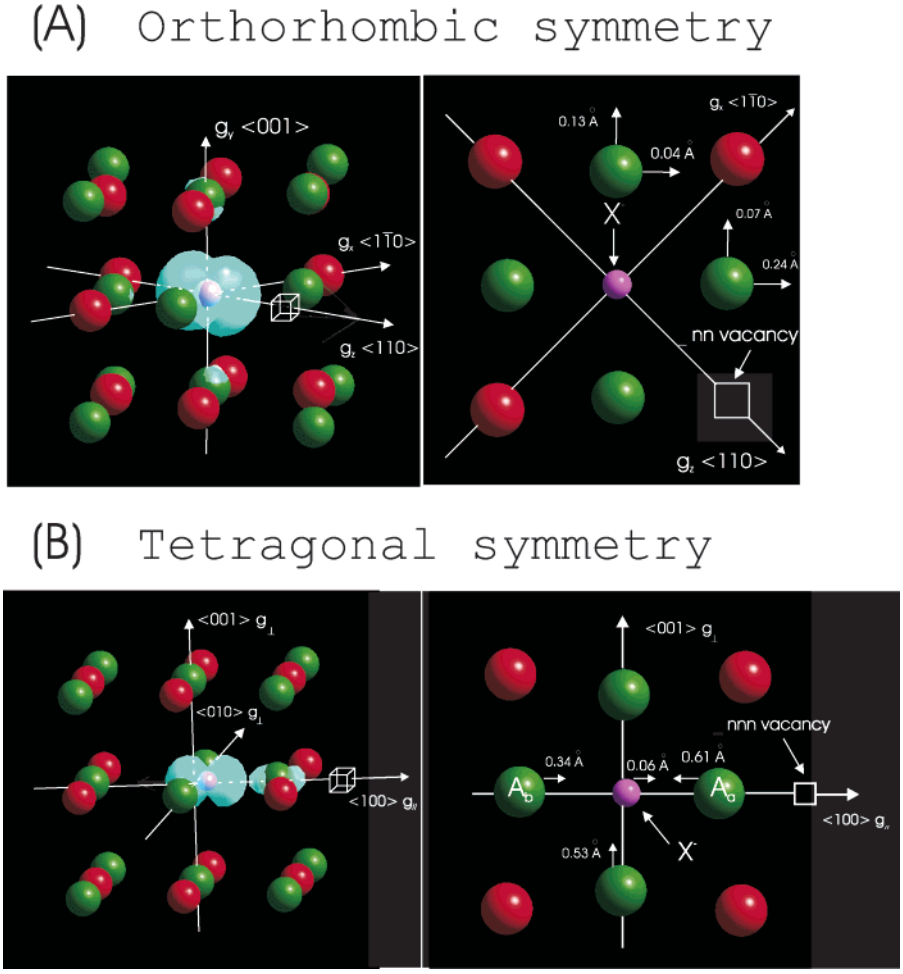

Figure 1. Substitutional defect models for X^- centers in MZ lattices: (A) nearest neighbor halide vacancy configuration (orthorhombic-I symmetry) in three dimensions (left) and cross section in the (001) plane (right). Unpaired spin density (left) and displacement of the central ion and first neighboring shell (right) are illustrated for the KCl:S^- defect structure. (B) Next nearest neighbor halide vacancy configuration (tetragonal symmetry) in three dimensions (left) and cross section in the (100) plane (right). Spin density (left) and optimized geometry (right) are shown for the KCl:O^-. The geometry relaxations for both the nn and nnn defect structures were obtained using an 87 cluster in vacuo and relaxing the nearest four lattice shells. The M^+ ions are colored green, and the Z^- are colored red. Halide vacancies are visualized as cubes. The unpaired spin density is visualized by a "blue" orbital.

TABLE 1: Composition and Definition of the Cluster Shells

shell	member	sublattice	no. of sites	shell	member	sublattice	no. of sites
1	100	M^+	6	19	411	Z^-	24
2	110	Z^-	12	20	331	M^+	24
3	111	M^+	8	21	420	Z^-	24
4	200	Z^-	6	22	421	M^+	48
5	210	M^+	24	23	332	Z^-	24
6	211	Z^-	24	24	422	Z^-	24
7	220	Z^-	12	25	430	M^+	24
8	221	M^+	24	26	500	M^+	6
9	300	M^+	6	27	431	Z^-	48
10	310	Z^-	24	28	333	M^+	8
11	311	M^+	24	29	432	M^+	48
12	222	Z^-	8	30	440	Z^-	12
13	320	M^+	24	31	441	M^+	24
14	321	Z^-	48	32	433	Z^-	24
15	400	Z^-	6	33	442	Z^-	24
16	322	M^+	24	34	443	M^+	24
17	410	M^+	24	35	444	Z^-	8
18	330	Z^-	12				

When performing embedded cluster calculations, the criterion about low total charge of the quantum cluster can be omitted since the total charge of the quantum cluster is compensated by the surrounding point charges. For computational feasibility reasons, only the 63 and 87 clusters will be tested in a two- and three-layered embedding scheme.

TABLE 2: Shell Composition (SC), Total Charge of the Defect Free Cluster (Q), and Madelung Constant (MC) for Different Cluster Sizes, with NOA the Number of Atoms in the Used Cluster

SC	NOA	Q	MC
1 → 4	33	−5	−0.867
1 → 5, 9	63	25	11.866
1 → 6, 9	87	1	2.068
1 → 8, 12	125	−1	1.561
1 → 12, 15	185	−1	1.663
1 → 20, 23, 26, 28	403	1	1.776

3.2. Approximation Schemes for Modeling Defects in a Lattice Environment. Defects in an ionic lattice environment can be modeled by various computational methods. The most widely used schemes are as follows: (i) a cluster in vacuo approximation, (ii) an embedded cluster model, and (iii) periodic calculations. All three schemes approximate the real extended system and have their specific advantages and disadvantages. An elaborate study on this item was recently performed by Mysovsky and co-workers.[61] We briefly summarize the main ideas of each approximation scheme below.

In **the cluster in vacuo approximation**, one uses a quantum mechanical cluster which is part of the bulk and is simply placed in a vacuum. This approach is only successful if the defect is embedded in a sufficiently large cluster, to allow proper

geometry relaxations.[6−11,62−65] When studying extended defects, as encountered here, the main drawback is the large computational cost associated with the large clusters as embedding is accounted on a quantum mechanical basis. The largest quantum cluster used in this work contains 403 atoms.

In the **embedded cluster model**, a quantum mechanical cluster is embedded in a finite array of point charges located at the lattice sites. There exist some variations of this concept in the literature. Sushko, Shluger, and Catlow developed a three region model in which the quantum part is surrounded by polarizable ions which are described in the shell model.[51] In the shell model, an ion is represented by a point core and shell connected by a spring to simulate its dipole polarizability. The positions of the cores and shells of each of these ions are optimized in response to the changes in the charge density distribution within the quantum cluster to minimize the total energy of the whole system. The ions closest to the quantum cluster can interact not only among themselves but also with the quantum cluster ions by means of specified interatomic potentials. The third region consists of fixed nonpolarizable ions, which provide the correct electrostatic distribution in the quantum cluster and the second region. The main advantage of this method is that it allows us to include the full extent of the defect-induced lattice distortion at reasonable computational cost. This method has been applied to study transition metal complexes in alkali halide lattices[52] and defects in chloride hosts.[66] A more simplified version consists of working in a two-layered approach in which the inner quantum mechanical region is surrounded by fixed point charges to reproduce the correct electrostatic potential in the quantum region. In section 4, the validity of the cluster in vacuo and a two- and three-layered embedded cluster approach is tested for $KCl:S^-$.

The last, and probably the most natural way to simulate the lattice, is by performing **periodic calculations**. In this approach, the paramagnetic ion is properly embedded in the crystalline environment and boundary effects are eliminated by imposing periodic boundary conditions. It is however important to enlarge the unit cell artificially to prevent defects in neighboring lattice cells from being too close to each other.[10] For the substitutional X^- defects under study, a unit cell with a minimum size of 343 atoms should be selected, which is computationally unfeasible. Therefore, such calculations have not been performed here.

3.3. Nomenclature for the Various Computational Schemes. For transparency, it is useful to introduce a compact notation indicating unambiguously the cluster size, the software, and the approximation scheme that is used for the calculation. The general format of the notation is P(x_{QM}, x_{PI}, x_{PC}) where P stands for the program package that is used (ADF or G03), x_{QM} represents the number of atoms in the quantum region (layer I), x_{PI} is the number of atoms contained in layer II with the polarizable ions (PI), and x_{PC} is the number of atoms in the layer III consisting of fixed point charges (PC). The various layers are illustrated in Figure 2. For a cluster in vacuo, the parameters x_{PI} and x_{PC} are zero, whereas for a cluster embedded in one layer, x_{PI} is zero. To clarify the notation, we give some examples for the 87 cluster, which will appear to be relevant in sections 4 and 5:

(i) ADF(87,0,0) refers to an 87-atom cluster in vacuo calculation performed with the ADF program package (see Figure 2A). In all following ADF calculations, the nearest four lattice shells are allowed to relax.

(ii) ADF(87,0,642) refers to an ADF calculation in which the quantum cluster is embedded in one layer of fixed point charges (Figure 2B). The number of fixed point charges in the two-layered approach is obtained by constructing a cubic array of nine ions in each direction giving 729 positions. To obtain the real number of point charges included in layer III (in a two-layered approach, we will still refer to the point charges as layer III for consistency; in that case, layer II is not present), one must subtract x_{QM} from 729. In ADF, the possibility to optimize the quantum cluster in an array of fixed point charges is not implemented. Therefore, the geometries are obtained by first optimizing the quantum cluster in vacuo. Subsequent properties such as energies and EPR values are then calculated by embedding this fixed geometry into an array of point charges. In principle, this is not a proper way of embedding since the quantum cluster is not optimized with the inclusion of the point charges.

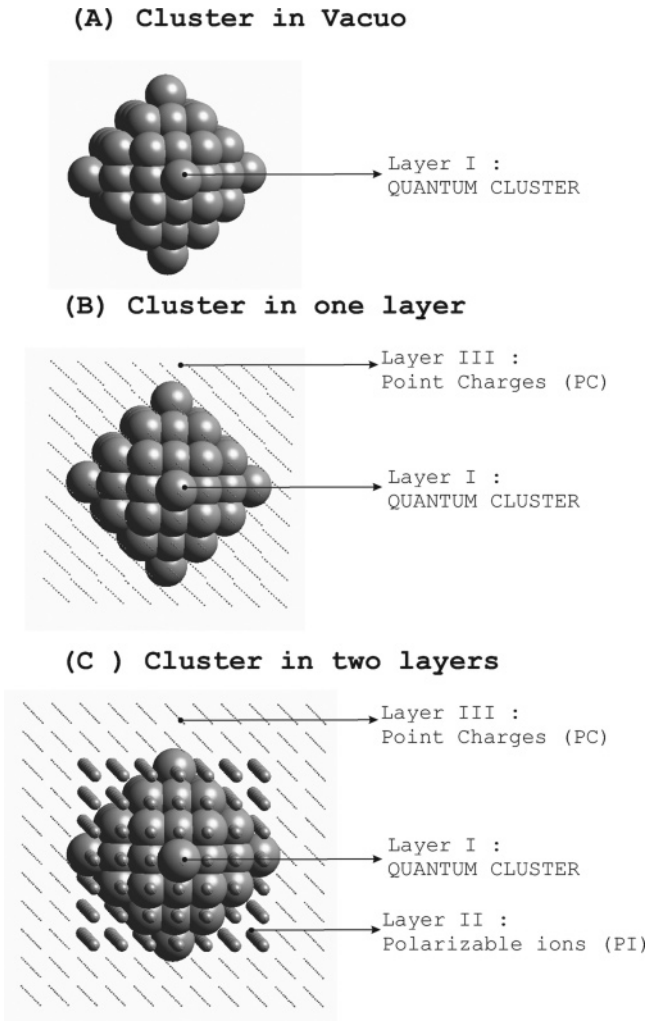

Figure 2. Illustration of (A) the cluster in vacuo model, (B) the two-layered embedded cluster model, and (C) the three-layered embedded cluster model.

(iii) G03(87,0,642) refers to a two-layered cluster calculation, as in the previous example. However, the optimization of the quantum cluster is performed properly within an array of point charges, as this option is implemented in G03.

(iv) G03(87,256,988) refers to a three-layered cluster calculation, using the GUESS code, in which 256 polarizable ions are considered in the second layer and 988 point charges in the third layer. The quantum cluster is optimized by fully accounting for the outer layers. The largest cubic array of point charges is obtained by including in each direction 11 atoms giving 1331 positions. The second layer is constructed by accounting for 7 atoms in each direction yielding 343 positions. By subtracting

TABLE 3: Energy Difference $\Delta E = E_{nn} - E_{nnn}$ (in eV) between the nn and nnn Vacancy Configurations as a Function of Cluster Size for the Substitutional KCl:S$^-$ Defect Structure[a]

	approximation scheme	size of quantum cluster (x_{QM})					
		33	63	87	125	185	403
	ADF(x_{QM},0,0)	10.940		−1.123	−1.175	−0.994	−0.904
ΔE	G03(x_{QM},0,0)[b]	6.809		−1.058			−0.911
exp: <0	ADF(x_{QM},0,729 − x_{QM})	1.305		−1.085	−1.101	−0.988	−0.903
	G03(x_{QM},0,729 − x_{QM})	5.357		−0.939			
	G03(x_{QM},343 − x_{QM}, 988)	2.583	−0.944	−0.927			
	ADF(x_{QM},0,0)	2.6114		2.6039	2.6037	2.6029	2.5584
g_x exp: 2.5436	ADF(x_{QM},0,729 − x_{QM})	2.6006		2.6009	2.6010	2.6005	
	G03(x_{QM},343 − x_{QM}, 988)		2.5954	2.5838			
	ADF(x_{QM},0,0)	2.1274		2.1686	2.1624	2.1601	2.1553
g_y exp: 2.2847	ADF(x_{QM},0,729 − x_{QM})	2.1263		2.1853	2.1893	2.1928	
	G03(x_{QM},343 − x_{QM}, 988)		2.1778	2.1672			
	ADF(x_{QM},0,0)	1.9207		1.9595	1.9528	1.9521	1.9532
g_z exp: 1.9073	ADF(x_{QM},0,729 − x_{QM})	1.9296		1.9350	1.9341	1.9301	
	G03(x_{QM},343 − x_{QM}, 988)		1.9403	1.9527			
	ADF(x_{QM},0,0)	110.1		106.9	106.8	106.9	124.8
A_x exp: 120	ADF(x_{QM},0,729 − x_{QM})	110.6		107.5	107.7	107.8	
	G03(x_{QM},343 − x_{QM}, 988)		160.28	159.9			
	ADF(x_{QM},0,0)	59.8		59.3	55.1	59.9	57.9
A_y exp: 58	ADF(x_{QM},0,729 − x_{QM})	60.3		57.6	58.2	58.4	
	G03(x_{QM},343 − x_{QM}, 988)		−53.31	−51.8			
	ADF(x_{QM},0,0)	88.2		89.3	88.1	88.7	82.9
A_z exp: 80	ADF(x_{QM},0,729 − x_{QM})	88.9		88.5	88.9	87.7	
	G03(x_{QM},343 − x_{QM}, 988)		−55.34	−53.1			

[a] Cluster in vacuo results are compared with embedded cluster data. Also, the g and hyperfine values (in MHz) are given. [b] The cluster in vacuo calculation labeled as G03(x_{QM},0,0) is obtained using the following procedure: (i) geometry optimization in ADF and (ii) energy calculation with G03 using geometry obtained in (i).

the number of atoms treated at a higher level (i.e., 343 in our example) from 1331, one gets the number of 988 as indicated in the shorthand notation. This example is clarified in Figure 2C.

4. Case Study: KCl:S$^-$

In this section, the S$^-$ center in KCl with orthorhombic-I g-tensor symmetry is taken as a test case to validate the various computational schemes for their accuracy in calculating energetic and spectroscopic properties. The final goal of this case study is the development of a computational flow scheme which can be applied to all X$^-$ centers under consideration at a reasonable computational cost. First, the influence of the cluster size and the applied simulation scheme on the energy difference between the vacancy configurations is investigated. For the lowest energy vacancy configuration, the sensitivity of EPR parameters calculations on the computational cluster model is investigated. As a last point, a general computational protocol is proposed which is feasible for all other MZ:X$^-$ defect structures.

4.1. Energetic Considerations. A stringent test for the computational protocol is the ability to predict the binding energy difference $\Delta E = E_{nn} - E_{nnn}$ between the nn and nnn vacancy configurations, reflecting their relative stabilities. If ΔE is negative, then an nn vacancy is energetically preferred; for a positive ΔE value, an nnn vacancy is favored. The ΔE values obtained for various cluster sizes and approximation schemes for KCl:S$^-$ are summarized in Table 3 and visualized in Figure 3. All clusters except the 33 cluster give negative values, indicating that the nn vacancy is the preferred defect configuration on energetic grounds. The deviant results for the 33 atoms cluster are related to cluster size effects, as the nnn vacancy is located at the edge of the quantum cluster and proper relaxation around the vacancy is not possible in this case. Embedding in an array of point charges does not solve this problem. The 403 cluster is the largest quantum cluster used in this study. It consists of 23 complete shells, and 135 atoms are allowed to relax. Such calculations are only feasible at high computational cost and on large workstations with parallel processing. For the cluster in vacuo results, the ΔE value appears to exhibit a complex dependence on the cluster size: it does not converge in a monotonic way. Embedded cluster calculations in ADF, that is, without optimization of the quantum cluster, hardly change the convergence behavior. The largest influence of embedding is noticed for the smallest clusters (87, 125) bringing the value to about −1.1 eV. As expected, the global effect of embedding reduces as the quantum cluster becomes larger. A proper way of embedding can in principle only be achieved by

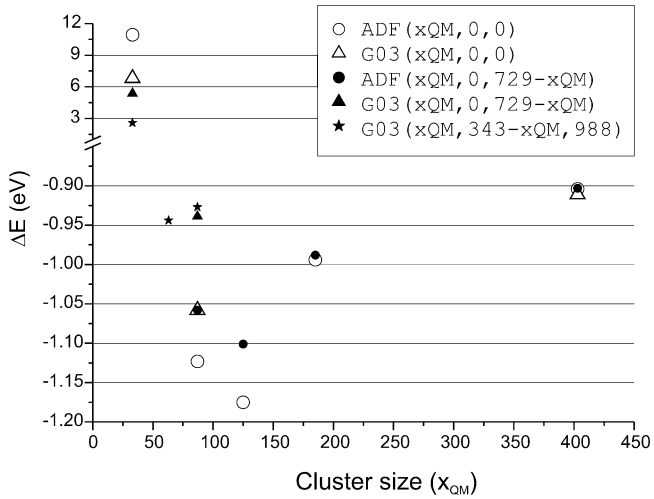

Figure 3. $\Delta E = E_{nn} - E_{nnn}$ values (in eV) obtained in various approximation schemes and for various cluster sizes for the KCl:S$^-$ defect system with orthorhombic-I g-tensor symmetry.

optimizing the quantum cluster in the presence of the array of point charges as is done in Gaussian. This procedure was followed for the 87 cluster. The energy value in the G03(87,0,-642) method amounts to −0.939 eV, approaching the value obtained at the G03(403,0,0) level quite closely (−0.911 eV). The effect of embedding in a three-layered scheme, where the quantum cluster is additionally surrounded by a shell of polarizable ions, brings the energy value (G03(87,256,988) = −0.927 eV) slightly closer to the G03(403,0,0) value. To reduce the computational cost, it is interesting to study the accuracy of the results obtained for the 63 cluster, which is properly embedded in an array of polarizable ions and point charges. The value for ΔE obtained at the G03(63,280,988) amounts to −0.944 eV. This 63 embedded cluster already gives acceptable energy differences. *Concluding, these results indicate that proper quantum embedding of the vacancies is necessary to obtain a qualitatively correct description of the stability of various vacancy configurations. Proper quantum embedding means that at least one shell of quantum atoms must surround the anion vacancy.* Moreover, to obtain accurate quantitative results, further embedding in point charges or quantum embedding is required. In our case, the smallest cluster fulfilling the requirement of quantum embedding of the vacancy contains 63 atoms. This rather small cluster is characterized by a high net charge in a vacuum, and adequate compensation by point charges is necessary.

Generally, all simulation schemes give preference for the nn position of the halide vacancy for the KCl:S^- test case and ΔE converges to −0.9 eV. This is in agreement with the experimentally observed orthorhombic-I *g*-tensor symmetry and may explain why the vacancy remains bound to the X^- ion, although its presence is not required for charge compensation. This defect model will now be tested in the reproduction of the EPR parameters.

4.2. EPR Parameters. A further test for the computational scheme and proposed defect model is the ability to reproduce qualitatively and if possible also quantitatively the experimental *g* and hyperfine tensors. Computed *g* and hyperfine values, using the cluster in vacuo and embedded cluster approach, for the KCl:S^- defect structure with an nn halide vacancy are compared with the available experimental data in Table 3. It should first of all be noted that for all cluster models qualitative agreement with experiment is obtained: the smallest (labeled g_z) and largest (labeled g_x) principal *g* values are found along ⟨110⟩ directions, and the smallest hyperfine value is found along the g_y axis. In the following, we will concentrate on the quantitative reproduction.

In Figure 4, the $\Delta g_i = g_i - g_e$ ($i = x, y, z$) values are plotted as a function of cluster size, using various schemes, together with the experimental data. At first sight, the Δg_i values tend to converge for the smaller clusters in vacuo. The deviations of these apparently converged values from experiment are still on the order of ≈0.1. To unravel the origin of this discrepancy, we found it instructive to perform an EPR calculation on the large 403 cluster in vacuo, despite the computational cost of such calculations. The result is very surprising in the sense that Δg_x now approaches the experimental value very closely, whereas Δg_y and Δg_z are practically unaltered and in less satisfactory agreement. Also, the three-layered embedded cluster (G03(63,-280,988)) calculations bring the g_x value in closer agreement with experiment, but the effect is rather minor. Analogously, the calculations on the 403 cluster in vacuo turn the principal *A* values in perfect agreement with experiment, although they had apparently already converged at smaller cluster sizes (see Table 3). On the other hand, the *A* values predicted in the three-layered embedded cluster model (in combination with Gaussian) exhibit a larger deviation from the experimental data, as compared with the ADF results (Table 3). The origin of this discrepancy is not clear and needs further investigation. In view of this, only hyperfine values obtained using ADF are taken into consideration in the further course of this paper.

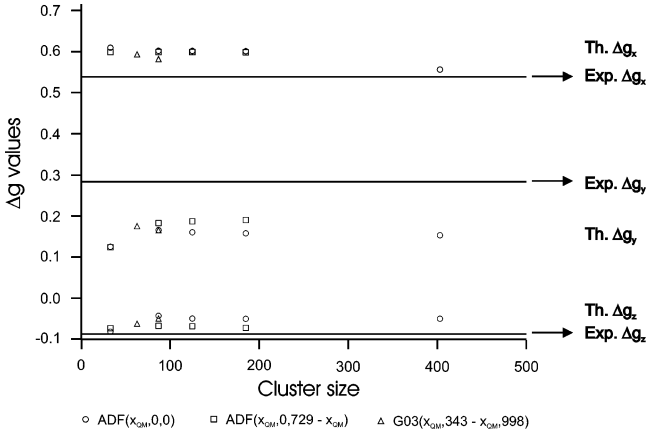

Figure 4. Influence of cluster size effects on the computed Δg values for the KCl:S^- defect structure with orthorhombic-I symmetry, using the various computational techniques. The experimental values are indicated as full lines.

TABLE 4: Computing Time for a Geometry Optimization of the Cluster in ADF and GUESS, Performed on an ALTIX 3300 Workstation with 12 CPUs and 2 GB RAM Per Processor

scheme	computer time
ADF(87,0,0)	3 days
ADF(403,0,0)	20 days
G03(87,256,988)	15 days

The substantial shift of Δg_x observed for the 403 cluster, at variance with Δg_y and Δg_z, deserves some special attention. Δg_x is by far the largest *g* shift, related to the important spin density in the plane perpendicular to the g_x axis (see Figure 4). The major fraction of this shift is due to spin−orbit interaction, which seems to be well described in this extended cluster model. The other contributions to the *g* factor are relatively less important for Δg_x, which might not be the case for Δg_y and Δg_z.

The significant improvement of g_x, A_x, A_y, and A_z for the 403 cluster suggests that to obtain quantitative agreement with experiment the size of the quantum cluster should be chosen large enough and/or that the calculated *g* and *A* tensors are very sensitive to relaxations of the lattice around the vacancy.

4.3. Selection of the Simulation Method. On the basis of the case study on KCl:S^-, it can be concluded that the best agreement between experimental and theoretical *g* and *A* values was obtained when using a 403 cluster in vacuo (ADF(403,0,0)), but its success should be seen in light of the computational cost. In Table 4, the computing time on 12 parallel CPUs in an Altix 3300 configuration with 2 GB RAM per processor is given. A calculation of all substitutional defect structures in MZ alkali halides that are subject of investigation in this work would need 250 days to perform all geometry optimizations and EPR calculations at the 403 cluster. In view of this, it is useful to search for a computationally attractive scheme which is feasible for all lattices under consideration and that gives correct qualitative and acceptable quantitative results.

The fact that various lattices contain heavy elements such as Rb or I further limits the options. For these elements, only a

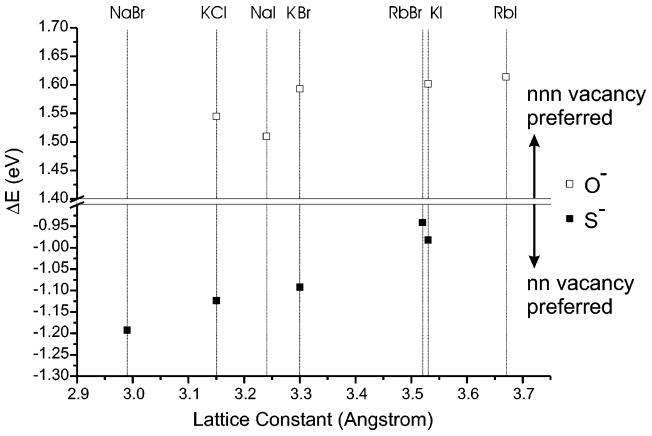

Figure 5. Energy difference (ΔE in eV) for the O^- and S^- defect structures for various lattices.

small part of all electron basis sets are available in Gaussian. The three-layered method, which has an interface with G03, is therefore less suited for lattices which contain these elements.

In addition to its low computational cost (see Table 4), the ADF(87,0,0) scheme is attractive in the following three respects:

(i) Simulation scheme: ADF is preferred over G03, because it better reproduces hyperfine tensors (see Table 3), and for all alkali and halide elements, accurate full electron basis sets are available.

(ii) ΔE values: The 87 cluster is the smallest cluster in vacuo which predicts the correct halide vacancy position. ΔE still deviates ≈0.2 eV (20%) from the value obtained for very large clusters in vacuo, but the qualitative picture does not change.

(iii) Reproduction of EPR parameters: Taking into account the very large deviations from the free electron value that are observed for the KCl:S^- defect structure (Δg: $-0.1 \rightarrow 0.6$), the 87 cluster gives very satisfactory quantitative agreement with experiment. The maximal deviation from the experimental g values is on the order of 0.1. Also, the principal A values are very well reproduced: maximum deviations of the order of 20% are observed.

In view of these features, the ADF(87,0,0) approach is selected for calculating the geometry, energy, and EPR parameters for the 11 MZ:X^- substitutional structures considered in this study. The good agreement between theory and experiment obtained in section 5 further justifies this choice.

5. Substitutional Models for X^- Centers in Alkali Halides: Computational Results and Discussion

In this section, we validate the substitutional models proposed in section 2 and illustrated in Figure 1 for the X^- centers with tetragonal and orthorhombic-I symmetry. First, energetic and geometric aspects are considered. On the basis of the convincing reproduction of g and (super)hyperfine tensors, the proposed models are finally accepted. The orthorhombic O^- defect in KBr emerges as an exception.

5.1. Energy and Geometry. If the defect models proposed in section 2 are correct, one expects that, for all substitutional X^- centers in MZ lattices, the vacancy configuration corresponding to the lowest energy will be experimentally encountered. If ΔE is small, the other configuration might occur as well. Figure 5 shows the ΔE values for the 10 MZ:X^- systems under study. In all cases, the calculated energy differences are so large that the overall qualitative picture will not change by increasing the cluster size or by choosing another way of embedding.

In all lattices, the O^- defects show a clear preference for an nnn vacancy configuration, while for the S^- defects, the nn configuration is energetically favored. It seems that the vacancy location is related to the size of the substituting chalcogen ion. Looking at the defect geometries, shown in Figure 1 for KCl:O^- and KCl:S^-, for all MZ lattices, the nearest cation shell is submitted to an inward relaxation if the Cl^- is replaced by the smaller O^- ion, and an outward relaxation in case of substitution by the larger S^- ion, both for the nn and for the nnn configurations. Furthermore, as a general trend, we find that for O^- defects $|\Delta E|$ increases with increasing lattice constant, whereas for S^- centers it decreases. In a theoretical study of T^{2+} ions on cation positions in alkali halides, Bannon et al.[46,47] reached similar conclusions: if the alkali ion is replaced by a smaller (larger) T^{2+} ion, then an nnn (nn) vacancy configuration is energetically preferred.

In KBr, both a tetragonal[20] and an orthorhombic-I[22] O^- center have been reported. The results in Figure 5 show a clear preference for the nnn vacancy configuration. $\Delta E \approx 1.6$ eV is of the same order of magnitude as that for the other MZ:O^- systems, where only the nnn vacancy configuration has been encountered. It is therefore highly questionable that only in this case a substitutional center with an nn vacancy would also exist. This indicates that another model should be proposed for this center. The calculated EPR parameters for this center further support such a hypothesis.

5.2. EPR Parameters for Tetragonal O^- Centers. A final test for the proposed model for these centers, a substitutional O^- ion with an nnn halide vacancy, is the reproduction of experimental g, hyperfine, and superhyperfine tensors. The computed and experimental g values are given in Table 5. In qualitative agreement with experiment, all calculated $g_{||}$ values are smaller and $g_\perp$ values are larger than the free electron value. This result can be understood by looking at the spin density for these centers, illustrated for KCl:O^- in Figure 1B. This spin density illustrates the lobe which contains the unpaired electron. As can be seen, the unpaired spin density is mainly localized along the ⟨100⟩ direction, which corresponds with the axis connecting the O^- ion and the halide vacancy. This is consistent with the fact that the ($g_{||}$) axis (smallest g value) corresponds with the direction of the paramagnetic lobe.[17] The quantitative agreement with experiment is also very satisfactory (maximum absolute deviation ≈0.1), although the calculations systematically underestimate $g_{||}$ and overestimate $g_\perp$.

The proposed defect structure can be further validated by comparing experimental and theoretical hyperfine (KI lattice) and superhyperfine data (KCl, KBr, and RbI lattices), also given in Table 5. The signs could be not determined from experiment for any of these couplings. For the KI:O^- defect structure, the ^{17}O hyperfine structure was measured and $A_{||}$ was found to be much larger than $A_\perp$. Our calculations nicely reproduce this experimental result, and even the quantitative agreement is quite good. For KCl, KBr, and RbI, a superhyperfine interaction with a single K or Rb nucleus was resolved in the EPR spectra. On the basis of this observation, it is expected that one of the nearest K or Rb nuclei on the ⟨100⟩ axis gives rise to this interaction. The computed superhyperfine data of the nearest A (A = K or Rb) nuclei located along the ⟨100⟩ axis, defined as A_a and A_b in Figure 1B, are compared with the experimental data in Table 5. The largest superhyperfine interaction is predicted for the alkali nucleus which is closest to the vacancy, while the calculated couplings of the other ions in the first shell (also those in the $g_\perp$ plane) are much smaller and only contribute to the line width of the EPR transitions. The agreement between

TABLE 5: Comparison between Theoretical and Experimental *g* Values for the Substitutional O^- Centers with a Vacancy on an nnn Halide Position[a]

		g tensor		hyperfine		superhyperfine			
						M_a		M_b	
lattice	comp	exp	theor.	exp	theor	exp	theor	exp	theor
NaI[b]	∥	1.9796	1.9099						
	⊥	2.2931	2.3752						
KCl[c]	∥	1.9800	1.9746			$\pm 25.0_{\pm 0.5}$	−23.4	n.a.	−3.3
	⊥	2.2580	2.3622			$\pm 12.0_{\pm 0.5}$	10.9	n.a.	1.9
KBr[d]	∥	1.9870	1.9717			$\pm 23_{\pm 1}$	−23.1	n.a.	−4.2
	⊥	2.2260	2.3228			$\pm 11_{\pm 1}$	9.1	n.a.	2.1
KI[b]	∥	1.9733	1.9071	$\pm 228_{\pm 5}$	192.7				
	⊥	2.3023	2.4097	$\pm 49_{\pm 2}$	−37.9				
RbI[b]	∥	1.9733	1.9576			$\pm 38_{\pm 4}$	−35.6	n.a.	−8.6
	⊥	2.2888	2.3686			$\pm 18_{\pm 2}$	16.9	n.a.	4.3

[a] Additionally, computed and experimental ^{17}O hyperfine ($KI:O^-$) and superhyperfine data for KCl, KBr (^{39}K), and RbI (^{85}Rb) (in MHz) are presented. Superhyperfine data for the nearest K and Rb nuclei along the ⟨100⟩ axis are also listed. The position of both nuclei is defined in Figure 1B. The error on the experimental data is given as a subscript. [b] Reference 22. [c] Reference 19. [d] Reference 20.

TABLE 6: Experimental and Theoretical *g* and Hyperfine Values (in MHz) for the S^- and the $KBr:O^-$ Centers with Orthorhombic-I Symmetry (*x*// ⟨110⟩, *y*// ⟨001⟩, *z*// ⟨110⟩) Using an nn Vacancy Defect Structure

	exp			theor			exp			theor		
defect	g_x	g_y	g_z	g_x	g_y	g_z	A_x	A_y	A_z	A_x	A_y	A_z
$NaBr:S^-$ [a]	2.4694	2.2705	1.9400	2.5727	2.1758	1.9878						
$KCl:S^-$ [a]	2.5436	2.2847	1.9073	2.6039	2.1686	1.9595	±120	±58	±80	106.9	59.3	89.3
$KBr:S^-$ [a]	2.6706	2.2876	1.8306	2.7709	2.1544	1.9041	±106	±83	±114	115.7	76.1	137.8
$KI:S^-$ [a]	2.7473	2.2023	1.8040	2.8568	2.1352	1.8695						
$RbBr:S^-$ [a]	2.7558	2.2567	1.7444	2.8854	2.1945	1.8124						
$KBr:O^-$ [b]	2.4416	2.2346	1.9508	2.2837	2.2078	1.8172	80.3	<75	214.5	130.8	75.2	138.9

[a] Reference 18. [b] Reference 22.

the experimental superhyperfine values and the computed data for the A_a nuclei is excellent in all cases.

The present calculations indeed strongly support our substitutional defect model with a vacancy on an nnn halide position for the X^- centers in alkali halides with tetragonal *g*-tensor symmetry.

5.3. EPR Parameters for Orthorhombic-I Centers. In Table 6, a comparison is made between experimental EPR values for the orthorhombic $MZ:X^-$ centers and corresponding theoretical results assuming a substitutional defect model with an nn halide vacancy. First, we concentrate on the results for the *g* tensor. As already noted in KCl (see section 4), for all S^- centers, the largest and smallest principal *g* values were found along the ⟨110⟩ directions. The deviations of the largest (g_x) and smallest (g_z) values from the free electron value are increasing as the lattice constant becomes larger, while the intermediate *g* value (g_y) is less affected. All these qualitative features are nicely reproduced by our calculations. Also quantitatively, the agreement between experimental and computed *g* values is very good (maximal absolute deviations ≈0.1). For all lattices, the calculations overestimate the experimental *g* values in the (001) plane, while the *g* value along the ⟨001⟩ axis is systematically underestimated. From experiment, it could not be determined whether the paramagnetic lobe, corresponding with the smallest *g* value, points toward the halide vacancy or whether it is orthogonal to the S^--vacancy axis. The calculations, on the other hand, provide a prompt answer to this question as seen in Figure 1A.

Also, computed ^{33}S hyperfine values are compared with available experimental data in Table 6. Again, the calculations perfectly reproduce the experimental trends: for both KCl and KBr, the smallest hyperfine value is directed along ⟨001⟩. Also, the direction of the largest principal *A* value, which is not the same for the two cases, is calculated in agreement with experiment. In addition, the quantitative agreement between experiment and theory is quite satisfactory.

On the basis of perfect qualitative and convincing quantitative correspondence between calculated and experimental EPR parameters, we conclude that the substitutional model with an nn halide vacancy is correct for the S^- centers with orthorhombic-I symmetry.

For the orthorhombic O^- center in KBr, the quantitative agreement is far worse than that for the S^- centers. In addition, an important qualitative discrepancy is noted for the hyperfine tensor. As for the S^- centers, the calculations predict that the principal values in the (001) plane are approximately equally large, while experimentally the A_z value turns out to be more than twice as large as A_x. Considering also the clear preference for an nnn vacancy for substitutional O^- in KBr (see Figure 5), we conclude that the substitutional defect model is inappropriate for this center. Brailsford and Morton[22] already made a preliminary suggestion of this kind, since the application of their specific doping procedure to other lattices (e.g., KCl, RbCl) unequivocally resulted in the occurrence of an interstitial defect. However, for this type of defect, the *g*-tensor symmetry is typically monoclinic-I and not orthorhombic-I. In a subsequent paper, we confirm the interstitial location of the O^- ion in this defect and show that its *g*-tensor symmetry only slightly (within experimental error) deviates from orthorhombic-I.

6. Conclusion

In this paper, we studied monoatomic X^- centers in alkali halide lattices with the principal aim to unravel the defect model that is able to predict the experimentally observed EPR parameters. The study was limited to X^- centers which exhibit tetragonal or orthorhombic-I *g*-tensor symmetry. As several of the proposed defect models are extended, that is, with vacancies at the nn and nnn positions, it was necessary to properly account

for the lattice environment. Various approximation schemes were tested on their ability to reproduce energy differences between various vacancy configurations and EPR parameters: *g* and hyperfine tensors. It was found that these properties are only converged when using very large quantum clusters. However, the qualitative behavior is already reproduced when working with smaller clusters (87, 185) in vacuo.

The following defect models are found to be valid:

(i) For the X^- centers with orthorhombic-I symmetry: a substitutional X^- ion with a vacancy on an nn halide position (cfr. Figure 1A).

(ii) For the X^- centers with tetragonal symmetry: a substitutional X^- ion with a vacancy on an nnn halide position (cfr. Figure 1B).

These conclusions are motivated by good qualitative and convincing quantitative reproduction of experimental *g*, hyperfine, and superhyperfine tensors. For all MZ:X^- systems under study, the experimentally encountered defect structure also corresponds to the energetically most stable vacancy configuration.

For the orthorhombic O^- center in KBr, neither of the considered models succeeds in reproducing the experimentally observed data. Most probably this center is located interstitially as suggested by Brailsford and Morton.[22] This specific item is further validated in part 2.

Acknowledgment. The authors (in particular V.V.S., H.V., and E.P.) would like to thank the Fund for Scientific Research (FWO-Flanders, Belgium) for financial support. The Research board of the Ghent University is also gratefully acknowledged.

References and Notes

(1) Florian, R.; Schwan, L. O.; Schmid, D. *Phys. Rev. A* **1984**, *29*, 2709.
(2) Kalachev, A. A.; Samartsev, V. V. *Laser Phys.* **2002**, *12*, 1114.
(3) Estreicher, S.; Estle, T. L. *Phys. Rev. B* **1984**, *30*, 7.
(4) Ewig, C. S.; Tellinghuisen, J. *J. Chem. Phys.* **1991**, *95*, 1097.
(5) Nishidate, K.; Baba, M.; Sarjono, S.; Hasegawa, M.; Nishikawa, K.; Sokolska, I.; Ryba-Romanowski, W. *Phys. Rev. B* **2003**, *68*, 224307.
(6) Stevens, F.; Vrielinck, H.; Callens, F.; Pauwels, E.; Waroquier, M. *Phys. Rev. B* **2002** *66*, 134103.
(7) Stevens, F.; Vrielinck, H.; Callens, F.; Pauwels, E.; Waroquier, M. *Phys. Rev. B* **2003**, *67*, 104429.
(8) Stevens; F.; Vrielinck, H.; Callens, F.; Waroquier, M. *Solid State Commun.* **2004**, *132*, 787.
(9) Stevens, F.; Van Speybroeck, V.; Pauwels, E.; Vrielinck, H.; Callens, F.; Waroquier, M. *Phys. Chem. Chem. Phys.* **2005**, *7*, 240.
(10) Van Speybroeck, V.; Pauwels, E.; Stevens, F.; Callens, F.; Waroquier, M. *Int. J. Quantum Chem.* **2005**, *101*, 761.
(11) Stevens, F.; Vrielinck, H.; Callens, F.; Pauwels, E.; Van Speybroeck, V.; Waroquier, M. *Int. J. Quantum Chem.* **2005**, *102*, 409.
(12) Känzig, W.; Cohen, M. H. *Phys. Rev. Lett.* **1959**, *3*, 509.
(13) Hausmann, A. *Z. Phys.* **1966**, *192*, 313.
(14) Schneider, J.; Dischler, B.; Räuber, A. *Phys. Status Solidi B* **1966**, *13*, 141.
(15) Suwalski, J.; Seidel, H. *Phys. Status Solidi* **1966**, *13*, 159.
(16) Zeller, H. R.; Känzig, W. *Helv. Phys. Acta* **1967**, *40*, 845.
(17) Shuey, R. T.; Zeller, H. R. *Helv. Phys. Acta* **1967**, *40*, 873.
(18) Vannotti, E.; Morton, J. R. *Phys. Rev.* **1968**, *174*, 448.
(19) Sander, W. *Z. Phys.* **1962**, *169*, 353.
(20) Sander, W. *Naturwissenschaften* **1964**, *51*, 404.
(21) Brailsford, J. R.; Morton, J. R.; Vannotti, E. *J. Chem. Phys.* **1968**, *49*, 2237.
(22) Brailsford, J. R.; Morton, J. R. *J. Chem. Phys.* **1969**, *51*, 4794.
(23) Matthys, P.; Callens, F.; Boesman, E. *Solid State Commun.* **1983**, *45*, 1.
(24) Callens, F.; Matthys, P.; Boesman, E. *Phys. Status Solidi B* **1983**, *118*, K35.
(25) Callens, F.; Maes, F.; Matthys, P.; Boesman, E. *J. Phys.: Condens. Matter* **1989**, *1*, 6921.
(26) Matthys, P.; Maes, F.; Callens, F.; Boesman, E. *Solid State Commun.* **1990**, *75*, 17.
(27) Maes, F.; Callens, F.; Matthys, P.; Boesman, E. *J. Phys. Chem. Solids* **1990**, *51*, 1289.
(28) Maes, F.; Callens, F.; Matthys, P.; Boesman, E. *Radiat. Eff. Defects Solids* **1991**, *116*, 283.
(29) Van Doorslaer, S.; Maes, F.; Callens, F.; Moens, P.; Boesman, E. *J. Chem. Soc., Faraday Trans.* **1994**, *90*, 2541.
(30) Van Doorslaer, S.; Callens, F.; Maes, F.; Matthys, P. *J. Phys.: Condens. Matter* **1995**, *7*, 1909.
(31) Van Doorslaer, S.; Callens, F.; Maes, F.; Boesman, E. *Phys. Rev. B* **1995**, *51*, 12480.
(32) Van Doorslaer, S.; Maes, F.; Callens, F.; Matthys, P.; Boesman, E. *J. Chem. Soc., Faraday Trans.* **1995**, *92*, 1579.
(33) Van Doorslaer, S.; Callens, F.; Maes, F.; Boesman, E.; Bouden, D. *Phys. Status Solidi B* **1996**, *196*, 213.
(34) Hennl, P. *Phys. Status Solidi B* **1977**, *84*, K151.
(35) Ashida, M.; Morikawa, O.; Arai, H.; Kato, R. *Prog. Cryst. Growth Charact. Mater.* **1996**, *33*, 105.
(36) Ye, R.; Tazawa, H.; Baba, M.; Nishidate, K.; Schwan, L. O.; Schmid, D. *Jpn. J. Appl. Phys. Part 2* **1998**, *37*, L1154.
(37) Ye, R.; Tazawa, H.; Baba, M.; Nishidate, K.; Schwan, L. O.; Schmid, D. *J. Lumin.* **2000**, *87*−*89*, 542.
(38) Wu, J.; Lin, J. *J. Cryst. Growth* **2002**, *240*, 495.
(39) Sarjono, S.; Baba, M.; Nishidate, K.; Ohta, K.; Sokolska, I.; Ryba-Romanowski, W. *Jpn. J. Appl. Phys.* **2004**, *43*, 3461.
(40) Alvares-Thon, L.; Hernandez-Acevedo, L.; Arratia-Perez, R. *J. Chem. Phys.* **2001**, *115*, 726.
(41) Foerster, S.; Stein, M.; Brecht, M.; Ogata, H.; Higuchi, Y.; Lubitz, W. *J. Am. Chem. Soc.* **2002**, *125*, 83.
(42) Arratia-Perez, R.; Hernandez-Acevedo, L. *J. Chem. Phys.* **2003**, *118*, 7425.
(43) Brownridge, S.; Grein, F. *J. Phys. Chem. A* **2003**, *107*, 7969.
(44) Aguado, A. *J. Phys. Chem. B* **2002**, *106*, 6991.
(45) Aguado, A. *J. Chem. Phys.* **2001**, *114*, 5256.
(46) Bannon, N. M.; Corish, J.; Jacobs, P. *Philos. Mag.* **1985**, *51*, 797.
(47) Bannon, N. M.; Corish, J.; Jacobs, P. *Philos. Mag.* **1985**, *52*, 61.
(48) Jahn, H. A.; Teller, E. *Proc. R. Soc. London, Ser. A* **1937**, *161*, 220.
(49) ADF, http://tc.chem.vu.nl/SCM, Department of Theoretical Chemistry, Vrije Universiteit Amsterdam.
(50) Frisch, M. J.; Trucks, G. W.; Schlegel, H. B.; Scuseria, G. E.; Robb, M. A.; Cheeseman, J. R.; Montgomery, J. A., Jr.; Vreven, T.; Kudin, K. N.; Burant, J. C.; Millam, J. M.; Iyengar, S. S.; Tomasi, J.; Barone, V.; Mennucci, B.; Cossi, M.; Scalmani, G.; Rega, N.; Petersson, G. A.; Nakatsuji, H.; Hada, M.; Ehara, M.; Toyota, K.; Fukuda, R.; Hasegawa, J.; Ishida, M.; Nakajima, T.; Honda, Y.; Kitao, O.; Nakai, H.; Klene, M.; Li, X.; Knox, J. E.; Hratchian, H. P.; Cross, J. B.; Adamo, C.; Jaramillo, J.; Gomperts, R.; Stratmann, R. E.; Yazyev, O.; Austin, A. J.; Cammi, R.; Pomelli, C.; Ochterski, J. W.; Ayala, P. Y.; Morokuma, K.; Voth, G. A.; Salvador, P.; Dannenberg, J. J.; Zakrzewski, V. G.; Dapprich, S.; Daniels, A. D.; Strain, M. C.; Farkas, O.; Malick, D. K.; Rabuck, A. D.; Raghavachari, K.; Foresman, J. B.; Ortiz, J. V.; Cui, Q.; Baboul, A. G.; Clifford, S.; Cioslowski, J.; Stefanov, B. B.; Liu, G.; Liashenko, A.; Piskorz, P.; Komaromi, I.; Martin, R. L.; Fox, D. J.; Keith, T.; Al-Laham, M. A.; Peng, C. Y.; Nanayakkara, A.; Challacombe, M.; Gill, P. M. W.; Johnson, B.; Chen, W.; Wong, M. W.; Gonzalez, C.; Pople, J. A. *Gaussian 03*, revision B.3; Gaussian, Inc.: Pittsburgh, PA, 2003.
(51) Sushko, P. V.; Shluger, A. L.; Catlow, C. R. A. *Surf. Sci.* **2000**, *450*, 153.
(52) Sushko, P. V.; Shluger, A. L.; Baetzold, R. C.; Catlow, C. R. A. *J. Phys.: Condens. Matter* **2000**, *12*, 8257.
(53) van Beest, B. W. H.; Kramer, G. J.; Santen, R. A. *Phys. Rev. Lett.* **1955**, *64*, 8.
(54) Sushko, P. V.; Mukhopadhyay, S.; Mysovsky, A. S.; Sulimov, V. B.; Taga, A.; Shluger, A. L. *J. Phys.: Condens. Matter* **2005**, *17*, S2115.
(55) Vosko, S. H.; Wilk, L.; Nusair, M. *Can. J. Phys.* **1980**, *58*, 1200.
(56) Becke, A. D. *Phys. Rev. A* **1988** *28*, 3098.
(57) Perdew, J. P. *Phys. Rev. B* **1986**, *33*, 8822.
(58) Herman, F.; Skilman, F. *Atomic Structure Calculations*; Prentice-Hall: Engelwood Cliffs, NJ, 1963.
(59) Rassolov, V.; Pople, J. A.; Ratner, M.; Windus, T. L. *J. Chem. Phys.* **1998**, *109*, 1223.
(60) Crandall, R. E. *Exp. Math.* **1999**, *8*, 367.
(61) Mysovsky, A. S.; Sushko, P. V.; Mukhopadhyay, S.; Edwards, A. H.; Shluger, A. L. *Phys. Rev. B* **2004**, *69*, 085202.
(62) Ewels, C. P.; Jones, R.; Oberg, S.; Miro, J.; Deak, P. *Phys. Rev. Lett.* **1996**, *77*, 865.
(63) Papanikolaou, N.; Zeller, R.; Dederichs, P. H.; Stefanou, N. *Comput. Mater. Sci.* **1997**, *8*, 131.
(64) Wissing, K.; Barriuso, M. T.; Aramburu, J. A.; Moreno, M. *J. Chem. Phys.* **1999**, *111*, 10217.
(65) Pauwels, E.; Van Speybroeck, V.; Lahorte, P.; Waroquier, M. *J. Phys. Chem. A* **2001**, *105*, 8794.
(66) Barandiaran, Z.; Seijo, L. *J. Chem. Phys.* **2003**, *119*, 3785.